Influence of Resonant Circuits on Optimal Design of Magnetostrictive Energy Harvester in Free Vibration

Yoshito Mizukawa, Jesse Ranta, Umair Ahmed, David Blažević, and Paavo Rasilo

Electrical Engineering Unit, Tampere University, 33720 Tampere, Finland

This article presents a novel modeling method for a magnetostrictive energy harvester connected to a resonant circuit. The method is based on analytical calculations coupled with experimental parameter identifications. The magnetic flux leakages from the pickup coil and the magnetostrictive material are considered. Under the assumptions of linearity and fundamental oscillation, the governing equations of the magnetostrictive energy harvester were derived from the Euler–Lagrange equations for an electromagnetic-mechanically coupled system. The energy-harvesting efficiency of the harvester was obtained by solving the derived governing equations, and it can be described with five non-dimensional parameters. Among the non-dimensional parameters, the natural frequency ratio and damping ratio of the load resistance have optimal values to maximize the energy-harvesting efficiency. This study derived these optimal design parameters depending on the circuit configuration and types of energy given to the harvester. In the magnetostrictive energy harvester with a series-resonant circuit subject to kinetic energy impact, these optimal design parameters can be obtained in simple algebraic forms. Experimental validations were conducted for the magnetostrictive energy harvester with a pure resistive circuit, with series- and parallel-resonant circuits, respectively, to compare their energy-harvesting efficiencies. While the pure resistive configuration can harvest 21% of given mechanical energy, both series- and parallel-resonant configurations can harvest 23%.

Index Terms— **Efficiency maximization, energy harvesting, free vibration, magnetostriction, primary damping, resonant circuit.**

I. Introduction

With the increasing number of structures such as bridges and buildings, manual inspection of those engineering structures has become progressively challenging. Monitoring structures with sensors enables efficient and objective safety assessments, thus gaining attention with the development of the Internet of Things and artificial intelligence. However, external power supply for sensors involves installation constraints or periodic battery replacement. Hence the principles and mechanisms of energy harvesting (i.e., capture and conversion of low-level ambient energy into electrical energy) have been actively studied [1], [2].

Vibration is the most ubiquitous energy source. Thus, vibration energy harvesting has a wide potential application area compared to other forms of environmental energy such as thermal or solar power, and has been expected to be embedded into monitoring systems. In recent years, frequency up-converting energy harvesters that can be applied to low-frequency environments have been developed [3], [4]. They convert the low-frequency excitation vibrations into impacts which in turn allow the energy-harvesting devices to oscillate at their natural frequencies often several times the excitation bandwidth. Priya [5] proposed a frequency up-converting piezoelectric wind turbine utilizing multiple piezoelectric cantilever harvesters. The rotational movement of the wind turbine is converted into oscillatory motion through a cam-shaft gear mechanism. Power is generated as the tips of the piezoelectric cantilever harvesters experience continuous impacts. Lin and Zhang [6] applied the frequency up-conversion to a wave energy conversion device. The device consists of a cylindrical buoy with teeth, and a strut that is mounted on the seabed and bears a box with an array of cantilever harvesters inside. As the buoy is excited by waves, the teeth slide along the strut and pluck the cantilever harvesters. Tan et al. [7] developed a frequency up-converting magnetostrictive energy harvester that harnesses power from human walking. A multi-leaf cam rotated by human footsteps through a gear rack repeatedly plucks the tip of the magnetostrictive cantilever harvester, thus coercing them to freely vibrate at their natural frequency.

Magnetostrictive energy harvesting utilizes the property of magnetostrictive materials in which the magnetic flux varies due to the applied mechanical force. This phenomenon is called the Villari effect. In contrast, the phenomenon where strain occurs when the magnetic flux within the material changes is known as the Joule effect, and it can be utilized for precise actuator mechanisms. Fe–Ga alloy is known as one of the giant magnetostrictive materials that exhibit large Villari effect and Joule effect. Fe–Ga alloy is frequently employed in magnetostrictive energy harvester mechanisms due to its high energy-harvesting efficiency, machinability, and environmental durability [8], [9], [10].

Many studies have been conducted on the optimization of vibration energy harvesters. Lefeuvre et al. [11] demonstrated that the rectifier with a buck-boost converter exhibits constant impedance. They modeled the charging circuit as a resistive load and optimized a piezoelectric energy harvester subject to harmonic excitation. Zuo and Cui [12] proposed an energy-harvesting tuned mass damper. They maximized the output power of the device subject to white-noise excitation. Palumbo et al. [13] experimentally investigated the optimal

Manuscript received 12 March 2024; revised 16 May 2024; accepted 10 June 2024. Date of publication 13 June 2024; date of current version 26 July 2024. Corresponding author: Y. Mizukawa (e-mail: yoshito.mizukawa@tuni.fi).

Color versions of one or more figures in this article are available at https://doi.org/10.1109/TMAG.2024.3413850.

Digital Object Identifier 10.1109/TMAG.2024.3413850

magnetic bias and optimal prestress with which the Fe–Ga alloy exhibits the largest magnetostrictive effect. We analytically derived the optimal resistance, optimal capacitance, and corresponding maximized output power of a magnetostrictive harvester subject to harmonic excitation [14]. We demonstrated that when the magnetostrictive harvester is connected to a resonant circuit, the output power is greater than that of a pure resistive circuit. Furthermore, we presented an analytical method for modeling cantilever-type magnetostrictive harvesters under mechanical impacts [15]. In the modeling, the shape function which is generally obtained by solving a complex frequency equation [16] was derived in a simple way based on the continuity of the magnetic flux inside the Fe–Ga alloy. Using the derived shape function, the algebraic optimal resistance to maximize the energy-harvesting efficiency was derived. However, the efficacy of a magnetostrictive energy harvester coupled with a resonant circuit subjected to mechanical impacts has not been elucidated. In addition, the magnetic flux leakage occurring in the harvester is neglected by the use of a closed magnetic circuit. An approach that takes into account the magnetic flux leakage is essential for general magnetostrictive energy harvesters.

In this article, we present a practical and generalized modeling method for a magnetostrictive energy harvester considering magnetic flux leakage and demonstrate that the magnetic flux leakage does not need to be considered by using the proposed experimental parameter identification method. Since this study directly identifies the parameters of the magnetostrictive energy harvester from experiments, the analytical modeling does not require the derivation of the shape function which involves strong approximations and complex calculations [15], [16]. The energy-harvesting efficiencies of the magnetostrictive energy harvesters with a series- and a parallel-resonant circuit are, respectively, derived. The optimal non-dimensional parameters, the corresponding optimal resistances, and the optimal capacitances to maximize the energy-harvesting efficiencies are proposed. In addition to the experimental parameter identification, experiments were conducted to validate the proposed method and optimal parameters.

II. Modeling Method

Fig. 1 shows the magnetostrictive energy harvester investigated in this study. The cantilever is composed of a Fe–Ga alloy laminated to an aluminum strip. Two magnets are attached to the fixed end and the free end of the cantilever to provide magnetic bias. A copper pickup coil is wound around the cantilever through a plastic bobbin for converting the energy of mechanically induced variations of the magnetic flux into electrical energy and thus achieve energy harvesting. In the charging circuit, a capacitor is connected in series with a load resistor to make a resonance in the circuit. The proposed method in this study relies on three assumptions which will be discussed in the following paragraphs.

A. Assumptions

The first assumption is that the induced oscillation is small enough for the magnetostrictive constitutive equations to be linear

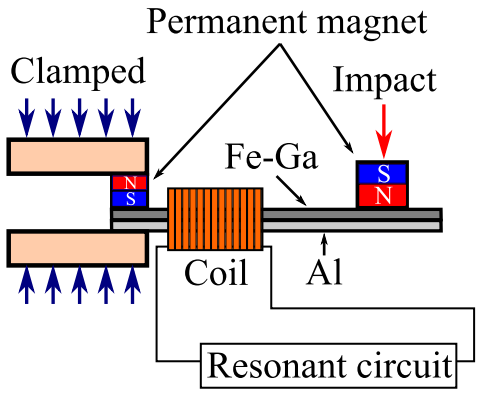

Fig. 1. Configuration of magnetostrictive energy harvester with resonant circuit.

$$H_i = \nu_{ij}^{\mathrm{S}} B_j - h_{ijk} S_{jk}$$
$$T_{ij} = -h_{kij} B_k + s_{ijkl}^{\mathrm{B}} S_{kl} \tag{1}$$

where H, T, B, and S are the variations of the magnetic field vector, stress tensor, magnetic flux density vector, and strain tensor in the Fe–Ga alloy, respectively. ν^{S}, s^{B}, and h are the magnetic reluctivity tensor at constant strain, elastic compliance tensor at constant magnetic flux density, and magnetostrictive constant tensor, respectively. The indices i, j, k, and l follow Einstein's summation convention. This assumption is often employed in analytical studies of magnetostrictive energy harvesters [14], [15], [16].

The second assumption is that the non-fundamental eigenmodes of the cantilever are negligible. In such cases, the displacement W of the cantilever, magnetic flux density B, and strain S can, respectively, be represented with separation of variables

$$W(x, y, z, t) = \psi_W(x, y, z) W_{\mathrm{mag}}(t)$$
$$B_i(x, y, z, t) = \psi_{Bi}(x, y, z) B_{\mathrm{mag}}(t)$$
$$S_{ij}(x, y, z, t) = \psi_{Sij}(x, y, z) S_{\text{Fe-Ga}}(t) \tag{2}$$

where the shape function ψ_W of the displacement W is normalized in such a way that the general displacement becomes equal to the displacement W_{mag} at the tip magnet. The shape function vector ψ_B is normalized in such a way that the general magnetic flux density becomes equal to the average magnetic flux density from the tip magnet, which satisfies the following relation:

$$\phi_{\mathrm{mag}}(t) = A_{\mathrm{mag}} B_{\mathrm{mag}}(t) \tag{3}$$

where ϕ_{mag} and A_{mag} are the magnetic flux from the tip magnet and the cross-sectional area of the tip magnet, respectively. The shape function tensor ψ_S is normalized so that the general strain becomes equal to the average strain in the Fe–Ga alloy.

Finally, we assume the linear assumption between the general displacement W_{mag} and the general strain $S_{\text{Fe-Ga}}$

$$W_{\mathrm{mag}}(t) = z_W S_{\text{Fe-Ga}}(t) \tag{4}$$

where z_W is a constant. It is noteworthy to mention that this assumption includes the Euler–Bernoulli beam assumption which is generally employed in the analytical modeling

of cantilever-type energy harvesters [15], [16], [17]. Therefore, this assumption is a less restrictive condition than the Euler–Bernoulli beam assumption.

B. System of Equations

The governing equations of the magnetostrictive energy harvester can be obtained from Euler–Lagrange equation

$$\frac{\mathrm{d}}{\mathrm{d}t}\left(\frac{\partial \mathcal{L}}{\partial \dot{q}_{\mathrm{gen}}(t)}\right) - \frac{\partial \mathcal{L}}{\partial q_{\mathrm{gen}}(t)} + \frac{\partial D}{\partial \dot{q}_{\mathrm{gen}}(t)} = 0 \tag{5}$$

where $\mathcal{L}$, D, and q_{gen} are Lagrangian, Rayleigh's dissipation function, and generalized coordinate, respectively. For an electromagnetic-mechanically coupled system, the Lagrangian $\mathcal{L}$ is represented with the kinetic energy K, energy of the inductor K_{e}, energy of the pickup coil K_{coil}, potential energy U, energy of the capacitor U_{e}, and magnetic energy U_{m} in the magnetostrictive energy harvester

$$\mathcal{L} = K + K_{\mathrm{e}} + K_{\mathrm{coil}} - U - U_{\mathrm{e}} - U_{\mathrm{m}}. \tag{6}$$

The kinetic energy of the harvester is obtained as follows:

$$\begin{aligned} K &= \frac{1}{2}\int_v \rho(x,y,z)\psi_W^2(x,y,z)\mathrm{d}v\dot{W}_{\mathrm{mag}}^2(t) \\ &= \frac{1}{2}m\dot{W}_{\mathrm{mag}}^2(t) \end{aligned} \tag{7}$$

where v, ρ, and m are the volume, mass density, and generalized mass of the cantilever including the pickup coil and tip magnet, respectively. The potential energy U is the sum of the strain energies of the Fe–Ga alloy $U_{\text{Fe-Ga}}$ and the aluminum strip U_{Al}

$$U = U_{\text{Fe-Ga}} + U_{\mathrm{Al}}. \tag{8}$$

The strain energies of the Fe–Ga alloy and aluminum strip are then expressed as

$$\begin{aligned} &U_{\text{Fe-Ga}} \\ &= \frac{1}{2}\int_v T_{ij}S_{ij}\mathrm{d}v \\ &= \frac{1}{2}\int_v \left(-h_{kij}B_k + s^B_{ijkl}S_{kl}\right)S_{ij}\mathrm{d}v \\ &= \frac{1}{2}\int_v s^{\mathrm{B}}_{ijkl}\psi_{Skl}(x,y,z)\psi_{Sij}(x,y,z)\mathrm{d}v S^2_{\text{Fe-Ga}}(t) \\ &\quad - \frac{1}{2}\int_v h_{kij}\psi_{Bk}(x,y,z)\psi_{Sij}(x,y,z)\mathrm{d}v B_{\mathrm{mag}}(t)S_{\text{Fe-Ga}}(t) \\ &= \frac{1}{2}\int_v \frac{s^{\mathrm{B}}_{ijkl}\psi_{Skl}(x,y,z)\psi_{Sij}(x,y,z)}{z_W^2}\mathrm{d}v W^2_{\mathrm{mag}}(t) \\ &\quad - \frac{1}{2}\int_v \frac{h_{kij}\psi_{Bk}(x,y,z)\psi_{Sij}(x,y,z)}{A_{\mathrm{mag}}z_W}\mathrm{d}v\phi_{\mathrm{mag}}(t)W_{\mathrm{mag}}(t) \\ &= \frac{1}{2}k_{\text{Fe-Ga}}W^2_{\mathrm{mag}}(t) - \frac{1}{2}\theta\phi_{\mathrm{mag}}(t)W_{\mathrm{mag}}(t) \\ &U_{\mathrm{Al}} \\ &= \frac{1}{2}k_{\mathrm{Al}}W^2_{\mathrm{mag}}(t) \end{aligned} \tag{9}$$

where θ is the magneto-mechanical coupling coefficient, and $k_{\text{Fe-Ga}}$ and k_{Al} are the generalized spring constants of the Fe–Ga alloy and aluminum strip, respectively.

To facilitate the understanding of the magnetic energy U_{m}, the magnetic fluxes appearing in the magnetostrictive energy harvester are shown in Fig. 2. The leakage flux ϕ_{leak1} is the magnetic flux leaking from the Fe–Ga alloy without passing through the pickup coil. The other leakage flux ϕ_{leak2} is the magnetic flux generated from the pickup coil which does not pass through the Fe–Ga alloy. In this case, the magnetic flux passing through both the Fe–Ga alloy and pickup coil is represented as $\phi_{\mathrm{mag}} - \phi_{\mathrm{leak1}}$. The combined reluctances corresponding to the magnetic fluxes $\phi_{\mathrm{mag}} - \phi_{\mathrm{leak1}}$, ϕ_{leak1}, and ϕ_{leak2} are defined as $\mathcal{R}$, $\mathcal{R}_1$, and $\mathcal{R}_2$, respectively. The reluctance of the magnet at the fixed end is included in the combined reluctance $\mathcal{R}$. Defining the magnetic energy of the Fe–Ga and the reluctance of the tip magnet as $U_{\mathrm{m,Fe\text{-}Ga}}$ and $\mathcal{R}_{\mathrm{mag}}$, respectively, the magnetic energy U_{m} of the magnetostrictive energy harvester is represented as follows:

$$\begin{aligned} U_{\mathrm{m}} &= U_{\mathrm{m,Fe\text{-}Ga}} + \frac{1}{2}\mathcal{R}\left(\phi_{\mathrm{mag}}(t) - \phi_{\mathrm{leak1}}(t)\right)^2 \\ &\quad + \frac{1}{2}\mathcal{R}_1\phi^2_{\mathrm{leak1}}(t) + \frac{1}{2}\mathcal{R}_2\phi^2_{\mathrm{leak2}}(t) + \frac{1}{2}\mathcal{R}_{\mathrm{mag}}\phi^2_{\mathrm{mag}}(t) \end{aligned} \tag{10}$$

where

$$\begin{aligned} U_{\text{Fe-Ga}} &= \frac{1}{2}\int_v H_i B_i \mathrm{d}v \\ &= \frac{1}{2}\int_v \left(\nu^{\mathrm{S}}_{ij}B_j - h_{ijk}S_{jk}\right)B_i\mathrm{d}v \\ &= \frac{1}{2}\int_v \nu^{\mathrm{S}}_{ij}\psi_{Bj}(x,y,z)\psi_{Bi}(x,y,z)\mathrm{d}v B^2_{\mathrm{mag}}(t) \\ &\quad - \frac{1}{2}\int_v h_{ijk}\psi_{Bi}(x,y,z)\psi_{Sjk}(x,y,z)\mathrm{d}v B_{\mathrm{mag}}(t)S_{\text{Fe-Ga}}(t) \\ &= \frac{1}{2}\int_v \frac{\nu^{\mathrm{S}}_{ij}\psi_{Bj}(x,y,z)\psi_{Bi}(x,y,z)}{A^2_{\mathrm{mag}}}\mathrm{d}v\phi^2_{\mathrm{mag}}(t) \\ &\quad - \frac{1}{2}\int_v \frac{h_{ijk}\psi_{Bi}(x,y,z)\psi_{Sjk}(x,y,z)}{A_{\mathrm{mag}}z_W}\mathrm{d}v\phi_{\mathrm{mag}}(t)W_{\mathrm{mag}}(t) \\ &= \frac{1}{2}\mathcal{R}_{\text{Fe-Ga}}\phi^2_{\mathrm{mag}}(t) - \frac{1}{2}\theta\phi_{\mathrm{mag}}(t)W_{\mathrm{mag}}(t) \end{aligned} \tag{11}$$

where $\mathcal{R}_{\text{Fe–Ga}}$ is the generalized reluctance of the Fe–Ga alloy. The energy of the pickup coil is given as follows [15]:

$$K_{\mathrm{coil}} = N\left(\phi_{\mathrm{mag}}(t) - \phi_{\mathrm{leak1}}(t) + \phi_{\mathrm{leak2}}(t)\right)\dot{q}(t) \tag{12}$$

where N and q are the number of turns in the pickup coil and the electric charge flowing in the pickup coil, respectively. Fig. 3 shows the small-signal magnetic circuit diagram of the magnetostrictive energy harvester. In small-signal analysis, the magnetomotive forces of the magnets are canceled out with the static components of the magnetic fluxes by the superposition theorem, thus they are omitted from the magnetic circuit diagram.

The energies in the electric circuit vary depending on whether it is series- or parallel-resonant. This section takes the series-resonant configuration as an example. In this case, the energies of an inductor and a capacitor are given as follows:

$$\begin{aligned} K_{\mathrm{e}} &= \frac{1}{2}L\dot{q}^2(t) \\ U_{\mathrm{e}} &= \frac{1}{2C}q^2(t) \end{aligned} \tag{13}$$

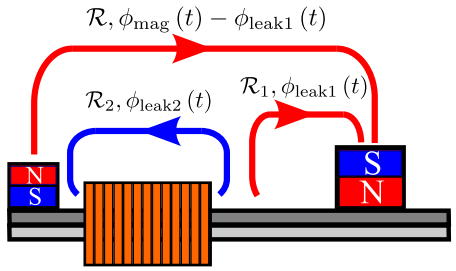

Fig. 2. Magnetic fluxes appearing in magnetostrictive energy harvester.

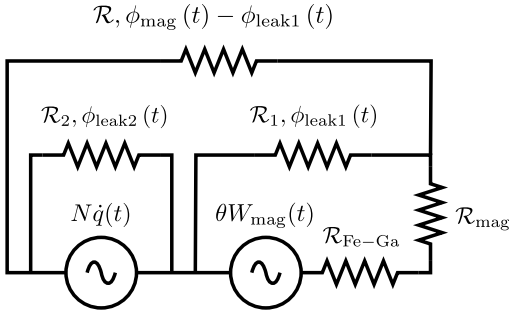

Fig. 3. Small-signal magnetic circuit diagram of magnetostrictive energy harvester.

where L and C are the external inductance and capacitance, respectively. In this study, there is no additional inductor in the circuit, and thus this inductance L is zero. However, for generality, this study considers the additional inductance.

The damping elements of the magnetostrictive energy harvester in this study are the primary damping with damping coefficient c, resistance R_{coil} of the pickup coil, and load resistance R. Thus, the Rayleigh's dissipation function D is given as follows:

$$D = \frac{1}{2}c\dot{W}_{\text{mag}}^2(t) + \frac{1}{2}R_{\text{coil}}\dot{q}^2(t) + \frac{1}{2}R\dot{q}^2(t). \tag{14}$$

From (5)–(14), the governing equations of the magnetostrictive energy harvester can be obtained as follows:

$$\begin{aligned}
&\frac{\mathrm{d}}{\mathrm{d}t}\left(\frac{\partial \mathcal{L}}{\partial \dot{W}_{\text{mag}}(t)}\right) - \frac{\partial \mathcal{L}}{\partial W_{\text{mag}}(t)} + \frac{\partial D}{\partial \dot{W}_{\text{mag}}(t)} \\
&\quad = m\ddot{W}_{\text{mag}}(t) + c\dot{W}_{\text{mag}}(t) + (k_{\text{Fe-Ga}} + k_{\text{Al}})W_{\text{mag}}(t) \\
&\qquad - \theta\phi_{\text{mag}}(t) = 0 \\
&\frac{\mathrm{d}}{\mathrm{d}t}\left(\frac{\partial \mathcal{L}}{\partial \dot{\phi}_{\text{mag}}(t)}\right) - \frac{\partial \mathcal{L}}{\partial \phi_{\text{mag}}(t)} + \frac{\partial D}{\partial \dot{\phi}_{\text{mag}}(t)} \\
&\quad = -\theta W_{\text{mag}}(t) + \left(\mathcal{R}_{\text{Fe-Ga}} + \mathcal{R}_{\text{mag}}\right)\phi_{\text{mag}}(t) \\
&\qquad + \mathcal{R}\left(\phi_{\text{mag}}(t) - \phi_{\text{leak1}}(t)\right) - N\dot{q}(t) = 0 \\
&\frac{\mathrm{d}}{\mathrm{d}t}\left(\frac{\partial \mathcal{L}}{\partial \dot{\phi}_{\text{leak1}}(t)}\right) - \frac{\partial \mathcal{L}}{\partial \phi_{\text{leak1}}(t)} + \frac{\partial D}{\partial \dot{\phi}_{\text{leak1}}(t)} \\
&\quad = -\mathcal{R}\left(\phi_{\text{mag}}(t) - \phi_{\text{leak1}}(t)\right) + \mathcal{R}_1\phi_{\text{leak1}}(t) + N\dot{q}(t) = 0 \\
&\frac{\mathrm{d}}{\mathrm{d}t}\left(\frac{\partial \mathcal{L}}{\partial \dot{\phi}_{\text{leak2}}(t)}\right) - \frac{\partial \mathcal{L}}{\partial \phi_{\text{leak2}}(t)} + \frac{\partial D}{\partial \dot{\phi}_{\text{leak2}}(t)} \\
&\quad = \mathcal{R}_2\phi_{\text{leak2}}(t) - N\dot{q}(t) = 0 \\
&\frac{\mathrm{d}}{\mathrm{d}t}\left(\frac{\partial \mathcal{L}}{\partial \dot{q}}\right) - \frac{\partial \mathcal{L}}{\partial q} + \frac{\partial D}{\partial \dot{q}} \\
&\quad = N\left(\dot{\phi}_{\text{mag}}(t) - \dot{\phi}_{\text{leak1}}(t) + \dot{\phi}_{\text{leak2}}(t)\right) \\
&\qquad + L\ddot{q}(t) + (R_{\text{coil}} + R)\dot{q}(t) + \frac{1}{C}q(t) = 0.
\end{aligned} \tag{15}$$

Eliminating the leakage magnetic fluxes ϕ_{leak1} and ϕ_{leak2} from (15) yields the following system of equations:

$$\begin{aligned}
&m\ddot{W}_{\text{mag}}(t) + c\dot{W}_{\text{mag}}(t) + (k_{\text{Fe-Ga}} + k_{\text{Al}})W_{\text{mag}}(t) \\
&\quad - \theta\phi_{\text{mag}}(t) = 0 \\
&\left[\mathcal{R}_{\text{Fe-Ga}} + \mathcal{R}_{\text{mag}} + \mathcal{R}\left(1 - \frac{\mathcal{R}}{\mathcal{R} + \mathcal{R}_1}\right)\right]\phi_{\text{mag}}(t) \\
&\quad - \theta W_{\text{mag}}(t) - N\left(1 - \frac{\mathcal{R}}{\mathcal{R} + \mathcal{R}_1}\right)\dot{q}(t) = 0 \\
&N\left(1 - \frac{\mathcal{R}}{\mathcal{R} + \mathcal{R}_1}\right)\dot{\phi}_{\text{mag}}(t) + \left(L + \frac{N^2}{\mathcal{R} + \mathcal{R}_1} + \frac{N^2}{\mathcal{R}_2}\right)\ddot{q}(t) \\
&\quad + (R_{\text{coil}} + R)\dot{q}(t) + \frac{1}{C}q(t) = 0.
\end{aligned} \tag{16}$$

For the parallel-resonant configuration, the governing equations are obtained as follows:

$$\begin{aligned}
&m\ddot{W}_{\text{mag}}(t) + c\dot{W}_{\text{mag}}(t) + (k_{\text{Fe-Ga}} + k_{\text{Al}})W_{\text{mag}}(t) \\
&\quad - \theta\phi_{\text{mag}}(t) = 0 \\
&\left[\mathcal{R}_{\text{Fe-Ga}} + \mathcal{R}_{\text{mag}} + \mathcal{R}\left(1 - \frac{\mathcal{R}}{\mathcal{R} + \mathcal{R}_1}\right)\right]\phi_{\text{mag}}(t) \\
&\quad - \theta W_{\text{mag}}(t) - N\left(1 - \frac{\mathcal{R}}{\mathcal{R} + \mathcal{R}_1}\right)\dot{q}(t) = 0 \\
&N\left(1 - \frac{\mathcal{R}}{\mathcal{R} + \mathcal{R}_1}\right)\dot{\phi}_{\text{mag}}(t) + \left(L + \frac{N^2}{\mathcal{R} + \mathcal{R}_1} + \frac{N^2}{\mathcal{R}_2}\right)\ddot{q}(t) \\
&\quad + R_{\text{coil}}\dot{q}(t) + \frac{1}{C}(q(t) - q_{\text{R}}(t)) = 0 \\
&\quad - \frac{1}{C}(q(t) - q_{\text{R}}(t)) + R\dot{q}_{\text{R}}(t) = 0
\end{aligned} \tag{17}$$

where q_{R} is the charge flowing through the resistive load.

Equations (16) and (17) take the same form as the governing equations for the model without considering magnetic flux leakage [15], and it can be seen that the leakage flux from the magnetostrictive material reduces the effective number of turns in the pickup coil, while the magnetic flux leakage from the pickup coil increases the inductance of the electric circuit. Fig. 4(a) and (b) shows the equivalent mechanical models of the magnetostrictive energy harvesters connected to a series-resonant circuit and a parallel-resonant circuit, respectively. Henceforth, the following substitutions are made for simplicity:

$$\begin{aligned}
k' &= k_{\text{Fe-Ga}} + k_{\text{Al}} \\
\mathcal{R}' &= \mathcal{R}_{\text{Fe-Ga}} + \mathcal{R}_{\text{mag}} + \mathcal{R}\left(1 - \frac{\mathcal{R}}{\mathcal{R} + \mathcal{R}_1}\right) \\
N' &= N\left(1 - \frac{\mathcal{R}}{\mathcal{R} + \mathcal{R}_1}\right) \\
L' &= L + \frac{N^2}{\mathcal{R} + \mathcal{R}_1} + \frac{N^2}{\mathcal{R}_2}.
\end{aligned} \tag{18}$$

III. Energy-Harvesting Efficiency of Magnetostrictive Energy Harvester

This section demonstrates the method to derive the energy-harvesting efficiency of the magnetostrictive energy harvester connected to a resonant circuit.

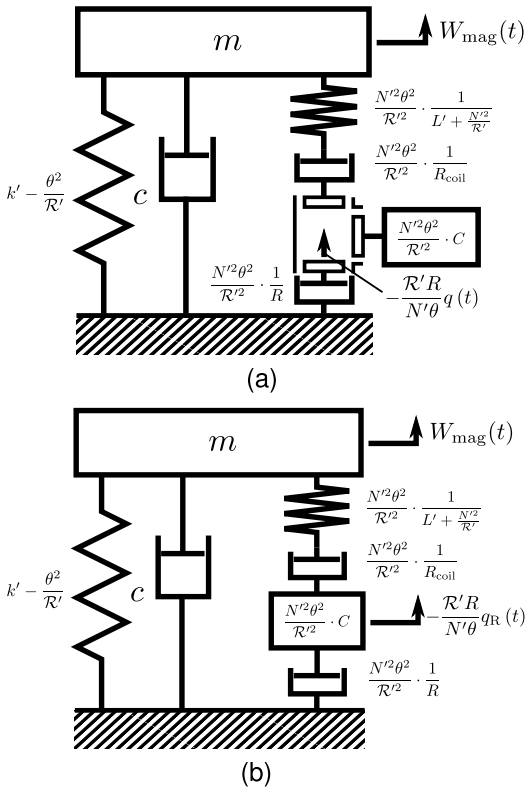

Fig. 4. Equivalent mechanical model of magnetostrictive energy harvester connected to a resonant circuit. (a) Series-resonant circuit. (b) Parallel-resonant circuit.

A. Series-Resonant Configuration

The dissipated energy Q from the load resistance R can be considered as harvestable energy [11], thus the energy-harvesting efficiency E can be defined as follows:

$$E = \frac{Q}{Q_{\mathrm{in}}} \tag{19}$$

where

$$\begin{aligned} Q &= \int_0^\infty \dot{q}^2(t) R \mathrm{d}t \\ Q_{\mathrm{in}} &= \frac{1}{2} m \dot{W}_{\mathrm{mag}}^2(0) + \frac{1}{2}\left(k' - \frac{\theta^2}{\mathcal{R}'}\right) W_{\mathrm{mag}}^2(0) \\ &\quad + \frac{1}{2}\left(L' + \frac{N'^2}{\mathcal{R}'}\right)\dot{q}^2(0) + \frac{1}{2C} q^2(0). \end{aligned} \tag{20}$$

In (19), Q_{in} is the initial state of energy given by impact. For energy-harvesting purposes, this study considers the energy-harvesting efficiency with respect to a given mechanical impact energy. Therefore, there is no energy in the inductor and capacitor at the initial state of the harvester ($\dot{q}(0) = q(0) = 0$).

The current $\dot{q}$ appearing in (20) can be obtained by solving the eigenvalue problem of (16) which can be represented as a matrix equation as

$$\boldsymbol{A}\boldsymbol{x} = \boldsymbol{0} \tag{21}$$

where

$$\begin{aligned} \boldsymbol{A} &= \begin{bmatrix} m\lambda^2 + c\lambda + k' & \theta & 0 \\ \theta & \mathcal{R}' & -N'\lambda \\ 0 & N'\lambda & L'\lambda^2 + (R_{\mathrm{coil}} + R)\lambda + \dfrac{1}{C} \end{bmatrix} \\ \boldsymbol{x} &= \begin{bmatrix} W_{\mathrm{mag}}(t) & \phi_{\mathrm{mag}}(t) & q(t) \end{bmatrix}^{\mathrm{T}} \end{aligned} \tag{22}$$

where λ is the complex eigenvalue. The complex eigenvalues can be obtained by solving the following characteristic equation:

$$\det \boldsymbol{A} = a_0\lambda^4 + a_1\lambda^3 + a_2\lambda^2 + a_3\lambda + a_4 = 0 \tag{23}$$

where

$$\begin{aligned} a_0 &= L'\mathcal{R}'m + N'^2 m \\ a_1 &= L'\mathcal{R}'c + N'^2 c + R\mathcal{R}'m + R_{\mathrm{coil}}\mathcal{R}'m \\ a_2 &= L'\mathcal{R}'k' - L'\theta^2 + N'^2 k' + R\mathcal{R}'c + R_{\mathrm{coil}}\mathcal{R}'c + \frac{\mathcal{R}'m}{C} \\ a_3 &= R\mathcal{R}'k' - R\theta^2 + R_{\mathrm{coil}}\mathcal{R}'k' - R_{\mathrm{coil}}\theta^2 + \frac{\mathcal{R}'c}{C} \\ a_4 &= \frac{\mathcal{R}'k'}{C} - \frac{\theta^2}{C}. \end{aligned} \tag{24}$$

Using the complex eigenvalues λ_1, λ_2, λ_3, and λ_4, the current $\dot{q}$ can be represented as follows:

$$\begin{aligned} \dot{q}(t) &= X_1\lambda_1 \exp(\lambda_1 t) + X_2\lambda_2 \exp(\lambda_2 t) \\ &\quad + X_3\lambda_3 \exp(\lambda_3 t) + X_4\lambda_4 \exp(\lambda_4 t) \end{aligned} \tag{25}$$

where

$$\begin{aligned} X_1 &= \frac{N'\theta}{L'\mathcal{R}' + N'^2}\frac{\lambda_1}{(\lambda_1-\lambda_2)(\lambda_1-\lambda_3)(\lambda_1-\lambda_4)}\dot{W}_{\mathrm{mag}}(0) \\ &\quad - \frac{N'\theta C}{\mathcal{R}'}\frac{\lambda_1\lambda_2\lambda_3\lambda_4}{(\lambda_1-\lambda_2)(\lambda_1-\lambda_3)(\lambda_1-\lambda_4)}W_{\mathrm{mag}}(0) \\ X_2 &= \frac{N'\theta}{L'\mathcal{R}' + N'^2}\frac{\lambda_2}{(\lambda_2-\lambda_3)(\lambda_2-\lambda_4)(\lambda_2-\lambda_1)}\dot{W}_{\mathrm{mag}}(0) \\ &\quad - \frac{N'\theta C}{\mathcal{R}'}\frac{\lambda_1\lambda_2\lambda_3\lambda_4}{(\lambda_2-\lambda_3)(\lambda_2-\lambda_4)(\lambda_2-\lambda_1)}W_{\mathrm{mag}}(0) \\ X_3 &= \frac{N'\theta}{L'\mathcal{R}' + N'^2}\frac{\lambda_3}{(\lambda_3-\lambda_4)(\lambda_3-\lambda_1)(\lambda_3-\lambda_2)}\dot{W}_{\mathrm{mag}}(0) \\ &\quad - \frac{N'\theta C}{\mathcal{R}'}\frac{\lambda_1\lambda_2\lambda_3\lambda_4}{(\lambda_3-\lambda_4)(\lambda_3-\lambda_1)(\lambda_3-\lambda_2)}W_{\mathrm{mag}}(0) \\ X_4 &= \frac{N'\theta}{L'\mathcal{R}' + N'^2}\frac{\lambda_4}{(\lambda_4-\lambda_1)(\lambda_4-\lambda_2)(\lambda_4-\lambda_3)}\dot{W}_{\mathrm{mag}}(0) \\ &\quad - \frac{N'\theta C}{\mathcal{R}'}\frac{\lambda_1\lambda_2\lambda_3\lambda_4}{(\lambda_4-\lambda_1)(\lambda_4-\lambda_2)(\lambda_4-\lambda_3)}W_{\mathrm{mag}}(0). \end{aligned} \tag{26}$$

The harvestable energy Q from the series-resonant circuit can be obtained as follows:

$$\begin{aligned} Q &= \int_0^\infty \dot{q}^2 R \mathrm{d}t \\ &= \frac{RN'^2\theta^2}{2\mathcal{R}^2\left(L'\mathcal{R}' + N'^2\right)^2}\frac{b_3}{b_1^2b_4 - b_1b_2b_3 + b_3^2}\dot{W}_{\mathrm{mag}}^2(0) \\ &\quad + \frac{RN'^2\theta^2C^2}{2\mathcal{R}'^2}\frac{b_1b_4^2}{b_1^2b_4 - b_1b_2b_3 + b_3^2}W_{\mathrm{mag}}^2(0) \end{aligned} \tag{27}$$

where b_1, b_2, b_3, and b_4 are the elementary symmetric polynomials

$$\begin{aligned} b_1 &= \lambda_1+\lambda_2+\lambda_3+\lambda_4 \\ b_2 &= \lambda_1\lambda_2+\lambda_1\lambda_3+\lambda_1\lambda_4+\lambda_2\lambda_3+\lambda_2\lambda_4+\lambda_3\lambda_4 \\ b_3 &= \lambda_1\lambda_2\lambda_3+\lambda_1\lambda_2\lambda_4+\lambda_1\lambda_3\lambda_4+\lambda_2\lambda_3\lambda_4 \\ b_4 &= \lambda_1\lambda_2\lambda_3\lambda_4. \end{aligned} \tag{28}$$

Equations (28) can be linked with (24) by Vieta's formulas

$$\begin{aligned} b_1 &= -\frac{a_1}{a_0} \\ b_2 &= \frac{a_2}{a_0} \\ b_3 &= -\frac{a_3}{a_0} \\ b_4 &= \frac{a_4}{a_0}. \end{aligned} \tag{29}$$

From (27) and (29), the harvestable energy Q can finally be obtained as

$$Q = \frac{1}{2}m\frac{\mathrm{Num_K}}{\mathrm{Den}}\dot{W}_{\mathrm{mag}}^2(0) + \frac{1}{2}\left(k' - \frac{\theta^2}{\mathcal{R}'}\right)\frac{\mathrm{Num_U}}{\mathrm{Den}}W_{\mathrm{mag}}^2(0) \tag{30}$$

where

$$\begin{aligned} \mathrm{Num_K} &= \kappa\nu^3\zeta_1\zeta_2+\kappa\nu^2\zeta_2^2+\kappa\nu\zeta_{\mathrm{coil}}\zeta_2 \\ \mathrm{Num_U} &= \kappa\nu\zeta_1\zeta_2+\kappa\nu^2\zeta_2^2+\kappa\nu\zeta_{\mathrm{coil}}\zeta_2 \\ \mathrm{Den} &= 4\,\nu^4{\zeta_1}^2{\zeta_2}^2+\nu^5\,\zeta_1\,\zeta_2+4\,\nu^3{\zeta_1}^3\,\zeta_2 \\ &\quad+8\,\nu^3\,{\zeta_1}^2\zeta_{\mathrm{coil}}\,\zeta_2+4\,\nu^3\zeta_1{\zeta_2}^3+\kappa\,\nu^3\zeta_1\,\zeta_2 \\ &\quad+\nu^4\zeta_1\,\zeta_{\mathrm{coil}}+4\,\nu^2\,{\zeta_1}^3\zeta_{\mathrm{coil}}+4\,\nu^2{\zeta_1}^2{\zeta_2}^2 \\ &\quad+4\,\nu^2{\zeta_1}^2{\zeta_{\mathrm{coil}}}^2+12\,\nu^2\zeta_1\,\zeta_{\mathrm{coil}}\,{\zeta_2}^2+\kappa\nu^2{\zeta_1}^2 \\ &\quad+\kappa\,\nu^2\zeta_1\,\zeta_{\mathrm{coil}}+\kappa\nu^2{\zeta_2}^2-2\nu^3\,\zeta_1\,\zeta_2 \\ &\quad+8\,\nu\,{\zeta_1}^2\zeta_{\mathrm{coil}}\,\zeta_2+12\,\nu\,\zeta_1\,{\zeta_{\mathrm{coil}}}^2\zeta_2+\kappa\,\nu\,\zeta_1\,\zeta_2 \\ &\quad+2\,\kappa\nu\,\zeta_{\mathrm{coil}}\,\zeta_2-2\,\nu^2\,\zeta_1\,\zeta_{\mathrm{coil}}+4\,{\zeta_1}^2{\zeta_{\mathrm{coil}}}^2 \\ &\quad+4\,\zeta_1{\zeta_{\mathrm{coil}}}^3+\kappa\,\zeta_1\,\zeta_{\mathrm{coil}}+\kappa{\zeta_{\mathrm{coil}}}^2+\nu\,\zeta_1\,\zeta_2+\zeta_1\zeta_{\mathrm{coil}}. \end{aligned} \tag{31}$$

The non-dimensional parameters in (31) are defined as follows: Electromagnetic-mechanical spring constant ratio

$$\kappa = \frac{N'^2\theta^2}{\mathcal{R}'^2\left(k'-\frac{\theta^2}{\mathcal{R}'}\right)\left(L'+\frac{N'^2}{\mathcal{R}'}\right)}$$

$$\text{Natural frequency ratio: } \nu = \frac{\omega_2}{\omega_1}$$

$$\text{Primary damping ratio: } \zeta_1 = \frac{c}{2m\omega_1}$$

$$\text{Damping ratio of coil resistance: } \zeta_{\mathrm{coil}} = \frac{R_{\mathrm{coil}}}{2\left(L'+\frac{N'^2}{\mathcal{R}'}\right)\omega_1}$$

$$\text{Damping ratio of load resistance: } \zeta_2 = \frac{R}{2\left(L'+\frac{N'^2}{\mathcal{R}'}\right)\omega_2} \tag{32}$$

where ω_1 and ω_2 are the undamped natural frequency of the mechanical-magnetic system and the electromagnetic system, respectively,

$$\begin{aligned} \omega_1 &= \sqrt{\frac{k'-\frac{\theta^2}{\mathcal{R}'}}{m}} \\ \omega_2 &= \frac{1}{\sqrt{\left(L'+\frac{N'^2}{\mathcal{R}'}\right)C}}. \end{aligned} \tag{33}$$

When impact vibration is induced only by either initial potential energy or initial kinetic energy, the energy-harvesting efficiency (19) is represented as follows:

$$\begin{aligned} E_{\mathrm{U}} &= \left.\frac{Q}{Q_{\mathrm{in}}}\right|_{\dot{W}_{\mathrm{mag}}(0)=0} = \frac{\mathrm{Num_U}}{\mathrm{Den}} \\ E_{\mathrm{K}} &= \left.\frac{Q}{Q_{\mathrm{in}}}\right|_{W_{\mathrm{mag}}(0)=0} = \frac{\mathrm{Num_K}}{\mathrm{Den}} \end{aligned} \tag{34}$$

where E_{U} and E_{K} are the energy-harvesting efficiency to potential energy input and kinetic energy input, respectively.

B. Parallel-Resonant Configuration

In the parallel-resonant circuit configuration, output energy Q and input energy Q_{in} are given as follows:

$$\begin{aligned} Q &= \int_0^\infty \dot{q}_{\mathrm{R}}^2(t)R\mathrm{d}t \\ Q_{\mathrm{in}} &= \frac{1}{2}m\dot{W}_{\mathrm{mag}}^2(0)+\frac{1}{2}\left(k'-\frac{\theta^2}{\mathcal{R}'}\right)W_{\mathrm{mag}}^2(0) \\ &\quad+\frac{1}{2}\left(L'+\frac{N'^2}{\mathcal{R}'}\right)\dot{q}^2(0)+\frac{1}{2C}(q(0)-q_{\mathrm{R}}(0))^2. \end{aligned} \tag{35}$$

In the initial state, there is no energy in the inductor and capacitor of the harvester ($\dot{q}(0) = q(0) - q_{\mathrm{R}}(0) = 0$). The current $\dot{q}_{\mathrm{R}}$ can be obtained by solving the eigenvalue problem (21) with

$$\begin{aligned} \boldsymbol{A} &= \begin{bmatrix} m\lambda^2+c\lambda+k' & \theta & 0 & 0 \\ \theta & \mathcal{R}' & -N'\lambda & 0 \\ 0 & N'\lambda & L'\lambda^2+R_{\mathrm{coil}}\lambda+\frac{1}{C} & -\frac{1}{C} \\ 0 & 0 & -\frac{1}{C} & R\lambda+\frac{1}{C} \end{bmatrix} \\ \boldsymbol{x} &= \begin{bmatrix} W_{\mathrm{mag}}(t) & \phi_{\mathrm{mag}}(t) & q(t) & q_{\mathrm{R}}(t) \end{bmatrix}^{\mathrm{T}}. \end{aligned} \tag{36}$$

The characteristic equation of (36) is given as

$$\det\boldsymbol{A} = a_0\lambda^4+a_1\lambda^3+a_2\lambda^2+a_3\lambda+a_4 = 0 \tag{37}$$

where

$$\begin{aligned} a_0 &= L'R\mathcal{R}'m+N'^2Rm \\ a_1 &= L'R\mathcal{R}'c+N'^2Rc+RR_{\mathrm{coil}}\mathcal{R}'m+\frac{L'\mathcal{R}'m}{C}+\frac{N'^2m}{C} \\ a_2 &= L'R\mathcal{R}'k'-L'R\theta^2+N'^2Rk'+RR_{\mathrm{coil}}\mathcal{R}'c+\frac{L'\mathcal{R}'c}{C} \\ &\quad+\frac{N'^2c}{C}+\frac{R\mathcal{R}'m}{C}+\frac{R_{\mathrm{coil}}\mathcal{R}'m}{C} \\ a_3 &= RR_{\mathrm{coil}}\mathcal{R}'k'-RR_{\mathrm{coil}}\theta^2+\frac{L'\mathcal{R}'k'}{C}-\frac{L'\theta^2}{C}+\frac{N'^2k'}{C} \end{aligned}$$

$$+\frac{R\mathcal{R}'c}{C}+\frac{R_{\mathrm{coil}}\mathcal{R}c}{C}$$
$$a_4=\frac{R\mathcal{R}'k'}{C}-\frac{R\theta^2}{C}+\frac{R_{\mathrm{coil}}\mathcal{R}'k'}{C}-\frac{R_{\mathrm{coil}}\theta^2}{C}. \tag{38}$$

Using the complex eigenvalues λ_1, λ_2, λ_3, and λ_4, the current $\dot{q}_{\mathrm{R}}$ can be represented as follows:

$$\dot{q}_{\mathrm{R}}(t)=X_1\lambda_1\exp(\lambda_1 t)+X_2\lambda_2\exp(\lambda_2 t)+X_3\lambda_3\exp(\lambda_3 t)+X_4\lambda_4\exp(\lambda_4 t) \tag{39}$$

where

$$X_1=\frac{N'\theta}{RC\left(L'\mathcal{R}'+N'^2\right)}\frac{1}{(\lambda_1-\lambda_2)(\lambda_1-\lambda_3)(\lambda_1-\lambda_4)}\dot{W}_{\mathrm{mag}}(0)-\frac{N'\theta}{\mathcal{R}'(R_{\mathrm{coil}}+R)}\frac{\lambda_2\lambda_3\lambda_4}{(\lambda_1-\lambda_2)(\lambda_1-\lambda_3)(\lambda_1-\lambda_4)}W_{\mathrm{mag}}(0)$$
$$X_2=\frac{N'\theta}{RC\left(L'\mathcal{R}'+N'^2\right)}\frac{1}{(\lambda_2-\lambda_3)(\lambda_2-\lambda_4)(\lambda_2-\lambda_1)}\dot{W}_{\mathrm{mag}}(0)-\frac{N'\theta}{\mathcal{R}'(R_{\mathrm{coil}}+R)}\frac{\lambda_1\lambda_3\lambda_4}{(\lambda_2-\lambda_3)(\lambda_2-\lambda_4)(\lambda_2-\lambda_1)}W_{\mathrm{mag}}(0)$$
$$X_3=\frac{N'\theta}{RC\left(L'\mathcal{R}'+N'^2\right)}\frac{1}{(\lambda_3-\lambda_4)(\lambda_3-\lambda_1)(\lambda_3-\lambda_2)}\dot{W}_{\mathrm{mag}}(0)-\frac{N'\theta}{\mathcal{R}'(R_{\mathrm{coil}}+R)}\frac{\lambda_1\lambda_2\lambda_4}{(\lambda_3-\lambda_4)(\lambda_3-\lambda_1)(\lambda_3-\lambda_2)}W_{\mathrm{mag}}(0)$$
$$X_4=\frac{N'\theta}{RC\left(L'\mathcal{R}'+N'^2\right)}\frac{1}{(\lambda_4-\lambda_1)(\lambda_4-\lambda_2)(\lambda_4-\lambda_3)}\dot{W}_{\mathrm{mag}}(0)-\frac{N'\theta}{\mathcal{R}'(R_{\mathrm{coil}}+R)}\frac{\lambda_1\lambda_2\lambda_3}{(\lambda_4-\lambda_1)(\lambda_4-\lambda_2)(\lambda_4-\lambda_3)}W_{\mathrm{mag}}(0). \tag{40}$$

The harvestable energy Q from the parallel-resonant circuit can be obtained as follows:

$$Q=\int_0^\infty \dot{q}_{\mathrm{R}}^2R\mathrm{d}t=\frac{N'^2\theta^2}{2RC^2\left(L'\mathcal{R}'+N'^2\right)^2}\frac{b_1}{b_1^2b_4-b_1b_2b_3+b_3^2}\dot{W}_{\mathrm{mag}}^2(0)+\frac{RN'^2\theta^2}{2\mathcal{R}'^2(R_{\mathrm{coil}}+R)^2}\frac{b_4(b_1b_2-b_3)}{b_1^2b_4-b_1b_2b_3+b_3^2}W_{\mathrm{mag}}^2(0). \tag{41}$$

Using Vieta's formulas (29) to (41), the harvestable energy (30) and energy efficiencies (34) for the parallel-resonant circuit configuration are obtained in which (31) is replaced with

$$\begin{aligned}\mathrm{Num_K}=\;&4\kappa\nu^4\zeta_{\mathrm{coil}}\zeta_2{}^3+\kappa\nu^5\zeta_2{}^2+4\kappa\nu^3\zeta_1\zeta_{\mathrm{coil}}\zeta_2{}^2\\&+4\kappa\nu^3\zeta_{\mathrm{coil}}{}^2\zeta_2{}^2+\kappa\nu^4\zeta_1\zeta_2+\kappa\nu^4\zeta_{\mathrm{coil}}\zeta_2\\ \mathrm{Num_U}=\;&4\kappa\nu^4\zeta_1\zeta_2{}^3+4\kappa\nu^4\zeta_{\mathrm{coil}}\zeta_2{}^3+\kappa\nu^5\zeta_2{}^2\\&+4\kappa\nu^3\zeta_1{}^2\zeta_2{}^2+8\kappa\nu^3\zeta_1\zeta_{\mathrm{coil}}\zeta_2{}^2\\&+4\kappa\nu^3\zeta_{\mathrm{coil}}{}^2\zeta_2{}^2+\kappa\nu^4\zeta_{\mathrm{coil}}\zeta_2+4\kappa\nu^2\zeta_1{}^2\zeta_{\mathrm{coil}}\zeta_2\\&+4\kappa\nu^2\zeta_1\zeta_{\mathrm{coil}}{}^2\zeta_2+\kappa^2\nu^2\zeta_1\zeta_2+\kappa^2\nu^2\zeta_{\mathrm{coil}}\zeta_2\\&+\kappa\nu^2\zeta_1\zeta_2\end{aligned}$$

$$\begin{aligned}\mathrm{Den}=\;&64\nu^3\zeta_1{}^2\zeta_{\mathrm{coil}}{}^2\zeta_2{}^4+64\nu^3\zeta_1\zeta_{\mathrm{coil}}{}^3\zeta_2{}^4\\&+16\kappa\nu^3\zeta_1\zeta_{\mathrm{coil}}\zeta_2{}^4+16\kappa\nu^3\zeta_{\mathrm{coil}}{}^2\zeta_2{}^4\\&+32\nu^4\zeta_1{}^2\zeta_{\mathrm{coil}}\zeta_2{}^3+48\nu^4\zeta_1\zeta_{\mathrm{coil}}{}^2\zeta_2{}^3\\&+64\nu^2\zeta_1{}^3\zeta_{\mathrm{coil}}{}^2\zeta_2{}^3+128\nu^2\zeta_1{}^2\zeta_{\mathrm{coil}}{}^3\zeta_2{}^3\\&+64\nu^2\zeta_1\zeta_{\mathrm{coil}}{}^4\zeta_2{}^3+4\kappa\nu^4\zeta_1\zeta_2{}^3\\&+8\kappa\nu^4\zeta_{\mathrm{coil}}\zeta_2{}^3+16\kappa\nu^2\zeta_1{}^2\zeta_{\mathrm{coil}}\zeta_2{}^3\\&+32\kappa\nu^2\zeta_1\zeta_{\mathrm{coil}}{}^2\zeta_2{}^3+16\kappa\nu^2\zeta_{\mathrm{coil}}{}^3\zeta_2{}^3\\&+4\nu^5\zeta_1{}^2\zeta_2{}^2+12\nu^5\zeta_1\zeta_{\mathrm{coil}}\zeta_2{}^2\\&+32\nu^3\zeta_1{}^3\zeta_{\mathrm{coil}}\zeta_2{}^2+64\nu^3\zeta_1{}^2\zeta_{\mathrm{coil}}{}^2\zeta_2{}^2\\&+16\nu^3\zeta_1\zeta_{\mathrm{coil}}\zeta_2{}^4+48\nu^3\zeta_1\zeta_{\mathrm{coil}}{}^3\zeta_2{}^2\\&+64\nu\zeta_1{}^3\zeta_{\mathrm{coil}}{}^3\zeta_2{}^2+64\nu\zeta_1{}^2\zeta_{\mathrm{coil}}{}^4\zeta_2{}^2\\&+\kappa\nu^5\zeta_2{}^2+4\kappa\nu^3\zeta_1{}^2\zeta_2{}^2+8\kappa\nu^3\zeta_1\zeta_{\mathrm{coil}}\zeta_2{}^2\\&+8\kappa\nu^3\zeta_{\mathrm{coil}}{}^2\zeta_2{}^2+32\kappa\nu\zeta_1{}^2\zeta_{\mathrm{coil}}{}^2\zeta_2{}^2\\&+32\kappa\nu\zeta_1\zeta_{\mathrm{coil}}{}^3\zeta_2{}^2+\nu^6\zeta_1\zeta_2+4\nu^4\zeta_1{}^3\zeta_2\\&+8\nu^4\zeta_1{}^2\zeta_{\mathrm{coil}}\zeta_2+4\nu^4\zeta_1\zeta_2{}^3+12\nu^4\zeta_1\zeta_{\mathrm{coil}}{}^2\zeta_2\\&+32\nu^2\zeta_1{}^3\zeta_{\mathrm{coil}}{}^2\zeta_2+16\nu^2\zeta_1{}^2\zeta_{\mathrm{coil}}\zeta_2{}^3\\&+32\nu^2\zeta_1{}^2\zeta_{\mathrm{coil}}{}^3\zeta_2+16\nu^2\zeta_1\zeta_{\mathrm{coil}}{}^2\zeta_2{}^3\\&+4\kappa^2\nu\zeta_1\zeta_{\mathrm{coil}}\zeta_2{}^2+4\kappa^2\nu\zeta_{\mathrm{coil}}{}^2\zeta_2{}^2\\&+\kappa\nu^4\zeta_{\mathrm{coil}}\zeta_2+12\kappa\nu^2\zeta_1{}^2\zeta_{\mathrm{coil}}\zeta_2\\&+12\kappa\nu^2\zeta_1\zeta_{\mathrm{coil}}{}^2\zeta_2+\nu^5\zeta_1\zeta_{\mathrm{coil}}+4\nu^3\zeta_1{}^3\zeta_{\mathrm{coil}}\\&+4\nu^3\zeta_1{}^2\zeta_2{}^2+4\nu^3\zeta_1{}^2\zeta_{\mathrm{coil}}{}^2-4\nu^3\zeta_1\zeta_{\mathrm{coil}}\zeta_2{}^2\\&+32\nu\zeta_1{}^2\zeta_{\mathrm{coil}}{}^2\zeta_2{}^2+16\nu\zeta_1\zeta_{\mathrm{coil}}{}^3\zeta_2{}^2\\&+\kappa^2\nu^2\zeta_1\zeta_2+\kappa^2\nu^2\zeta_{\mathrm{coil}}\zeta_2+\kappa\nu^3\zeta_1{}^2\\&+\kappa\nu^3\zeta_1\zeta_{\mathrm{coil}}+8\kappa\nu\zeta_1\zeta_{\mathrm{coil}}\zeta_2{}^2+4\kappa\nu\zeta_{\mathrm{coil}}{}^2\zeta_2{}^2\\&-2\nu^4\zeta_1\zeta_2+8\nu^2\zeta_1{}^2\zeta_{\mathrm{coil}}\zeta_2-4\nu^2\zeta_1\zeta_{\mathrm{coil}}{}^2\zeta_2\\&+16\zeta_1{}^2\zeta_{\mathrm{coil}}{}^3\zeta_2+16\zeta_1\zeta_{\mathrm{coil}}{}^4\zeta_2+2\kappa\nu^2\zeta_1\zeta_2\\&+\kappa\nu^2\zeta_{\mathrm{coil}}\zeta_2+4\kappa\zeta_1\zeta_{\mathrm{coil}}{}^2\zeta_2+4\kappa\zeta_{\mathrm{coil}}{}^3\zeta_2\\&-2\nu^3\zeta_1\zeta_{\mathrm{coil}}+4\nu\zeta_1{}^2\zeta_{\mathrm{coil}}{}^2+4\nu\zeta_1\zeta_{\mathrm{coil}}\zeta_2{}^2\\&+4\nu\zeta_1\zeta_{\mathrm{coil}}{}^3+\kappa\nu\zeta_1\zeta_{\mathrm{coil}}+\kappa\nu\zeta_{\mathrm{coil}}{}^2\\&+\nu^2\zeta_1\zeta_2+4\zeta_1\zeta_{\mathrm{coil}}{}^2\zeta_2+\nu\zeta_1\zeta_{\mathrm{coil}}\end{aligned} \tag{42}$$

where the damping ratio $\zeta_{2\mathrm{opt}}$ of the load resistance is redefined as

$$\zeta_2=\frac{\left(L'+\frac{N'^2}{\mathcal{R}'}\right)\omega_2}{2R} \tag{43}$$

for the parallel-resonant circuit.

IV. Efficiency Maximization

Among the non-dimensional parameters present in (32), the larger the κ is, the higher the energy-harvesting efficiencies become as shown in (34), while larger values of ζ_1 and ζ_{coil} result in lower efficiencies. The remaining two non-dimensional parameters, natural frequency ratio ν and damping ratio of the load resistance ζ_2, have optimal values for maximizing the energy-harvesting efficiency. These optimal parameters can be obtained by solving the following system

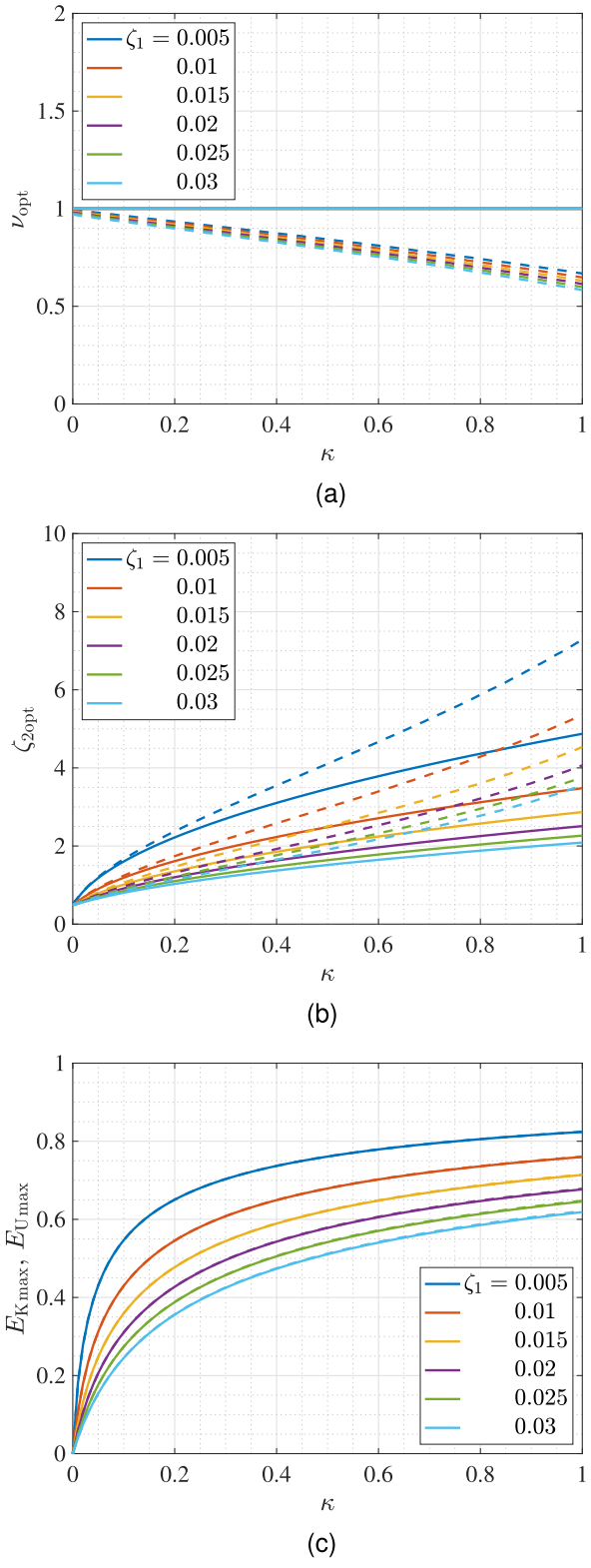

Fig. 5. Optimal parameters and maximized energy-harvesting efficiency to kinetic energy (solid line) and potential energy (dashed line) of magnetostrictive energy harvester connected to a series-resonant circuit with a variation of primary damping ratio ζ_1 ($\zeta_{\rm coil} = 0.4656$). (a) Optimal natural frequency. (b) Optimal damping ratio of load resistance. (c) Maximized energy-harvesting efficiency.

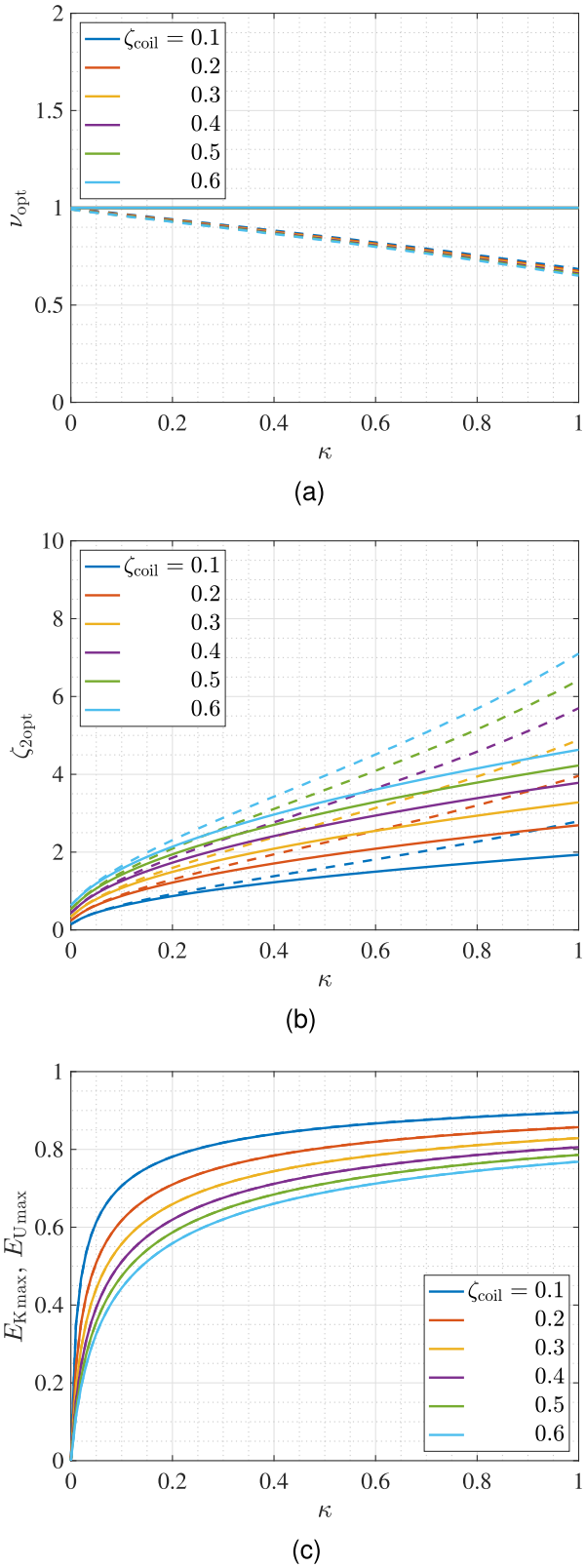

Fig. 6. Optimal parameters and maximized energy-harvesting efficiency to kinetic energy (solid line) and potential energy (dashed line) of magnetostrictive energy harvester connected to a series-resonant circuit with a variation of damping ratio $\zeta_{\rm coil}$ of coil resistance ($\zeta_1 = 0.0072$). (a) Optimal natural frequency. (b) Optimal damping ratio of load resistance. (c) Maximized energy-harvesting efficiency.

of equations:

$$\frac{\partial E}{\partial \nu} = 0$$

$$\frac{\partial E}{\partial \zeta_2} = 0. \tag{44}$$

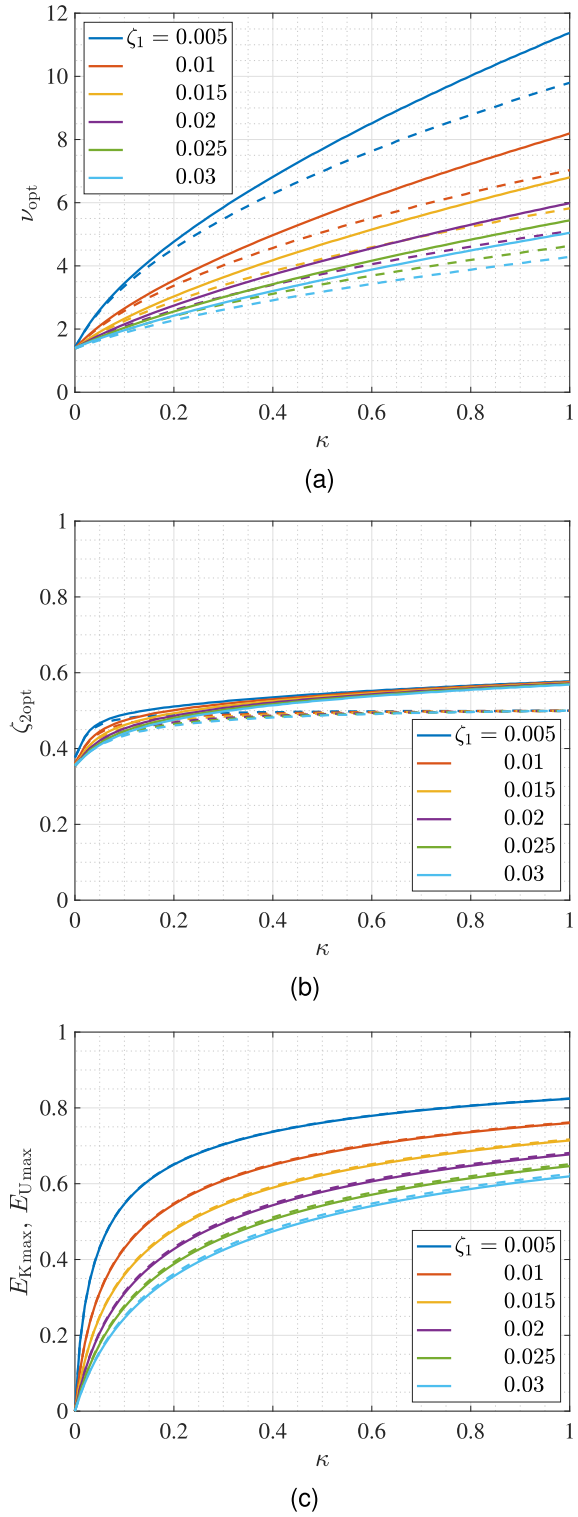

Fig. 7. Optimal parameters and maximized energy-harvesting efficiency to kinetic energy (solid line) and potential energy (dashed line) of magnetostrictive energy harvester connected to a parallel-resonant circuit with a variation of primary damping ratio ζ_1 ($\zeta_{\rm coil} = 0.4656$). (a) Optimal natural frequency. (b) Optimal damping ratio of load resistance. (c) Maximized energy-harvesting efficiency.

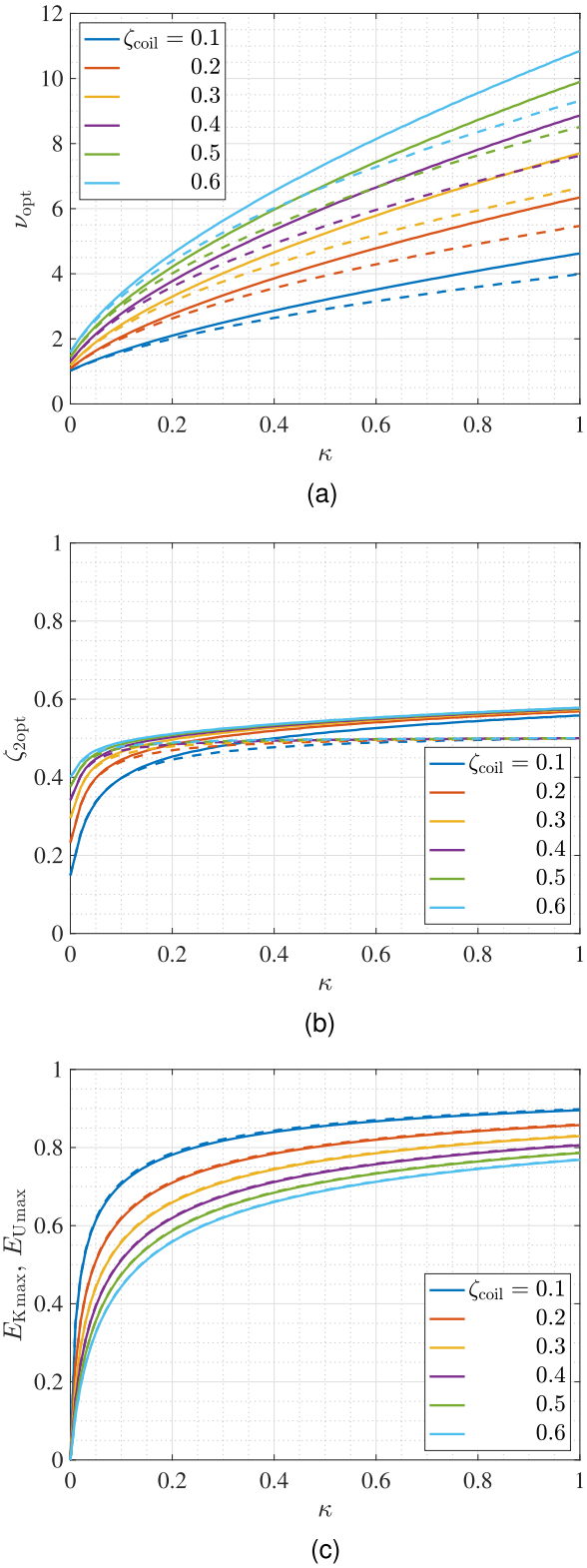

Fig. 8. Optimal parameters and maximized energy-harvesting efficiency to kinetic energy (solid line) and potential energy (dashed line) of magnetostrictive energy harvester connected to a parallel-resonant circuit with a variation of damping ratio $\zeta_{\rm coil}$ of coil resistance ($\zeta_1 = 0.0072$). (a) Optimal natural frequency. (b) Optimal damping ratio of load resistance. (c) Maximized energy-harvesting efficiency.

A. Maximized Efficiency of Magnetostrictive Energy Harvester With a Series-Resonant Circuit

Figs. 5 and 6 show the (a) optimal natural frequency ratio $\nu_{\rm opt}$, (b) optimal damping ratio $\zeta_{2\rm opt}$ of the load resistance, and (c) maximized energy-harvesting efficiency of the magnetostrictive energy harvester connected to a series-resonant circuit with a variation of the primary damping ratio ζ_1 and the

damping ratio ζ_{coil} of the coil resistance, respectively. While the optimal parameters to maximize the energy-harvesting efficiency to potential energy are solved numerically, the optimal parameters to maximize the energy-harvesting efficiency to kinetic energy can be obtained in the form of simple algebraic solutions as follows:

$$\nu_{\text{opt}} = 1$$
$$\zeta_{2\text{opt}} = \frac{\sqrt{\zeta_1(\zeta_1+\zeta_{\text{coil}})(4\zeta_1\zeta_{\text{coil}}+\kappa)}}{2\zeta_1}. \tag{45}$$

B. Maximized Efficiency of Magnetostrictive Energy Harvester With Parallel-Resonant Circuit

Figs. 7 and 8 show the numerically solved (a) optimal natural frequency ratio ν_{opt}, (b) optimal damping ratio $\zeta_{2\text{opt}}$ of the load resistance, and (c) maximized energy-harvesting efficiency of the magnetostrictive energy harvester connected to a parallel-resonant circuit with a variation of the primary damping ratio ζ_1 and the damping ratio ζ_{coil} of the coil resistance, respectively. Comparing the series- and parallel-resonant configurations, there is almost no difference between their maximized energy-harvesting efficiencies while their optimal design parameters take substantially different values. In addition, in each configuration, the optimal design parameters for kinetic and potential energy input are approximately equal for small κ and deviate from each other as κ increases. This means that, in series configuration, the algebraic optimal parameters (45) for kinetic energy input can approximately optimize the harvester even when the free vibration is induced by potential energy input. Therefore, even though the two configurations do not significantly differ in their harvestable energy, the series configuration is superior to the parallel configuration for the reason that the optimal design parameters of the series configuration are available as simple algebraic solutions.

V. Experimental Parameter Identification

Fig. 9 shows the magnetostrictive energy harvester designed and built for experiments. The cantilever is composed of a 1.0 × 6.0 × 60 mm Fe–Ga strip and an aluminum strip of equal dimensions laminated together by superglue. A pickup coil is built from enameled copper wire with a diameter of 0.10 mm and is wound around a plastic bobbin with a thickness of 1.0 mm. The number of turns in the coil and the resistance of the coil are 2000 and 142 Ω, respectively. A 10-mm cubic neodymium magnet is mounted 6 mm from the free end of the cantilever. A 6.0-mm cubic neodymium magnet is attached to the fixed end of the cantilever and clamped together with the cantilever by a vise.

As seen from (32), (33), and (43), to obtain the analytical energy-harvesting efficiency with known R_{coil}, R, and C, the natural frequency ω_1 and damping ratio ζ_1 of the cantilever, inductance $L' + (N'^2/\mathcal{R}')$, and electromagnetic-mechanical spring constant ratio κ need to be identified from experiments. The natural frequency ω_1 and damping ratio ζ_1 of the cantilever were measured by the free vibration experiment shown in Fig. 10(a). A 100 g weight was hung on the magnet at the free end by a copper wire with a diameter of 0.05 mm. When the copper wire breaks, free vibration is induced due to the potential energy given by the weight. The induced voltage between the pickup coil was measured by a data acquisition device (NI USB-6251 from National Instruments). Fig. 10(b) shows the obtained open-circuit free voltage response. From the period of the damped oscillation and the logarithmic decrement, $\omega_1 = 1502$ rad s^{-1} and $\zeta_1 = 0.0072$ were calculated, respectively.

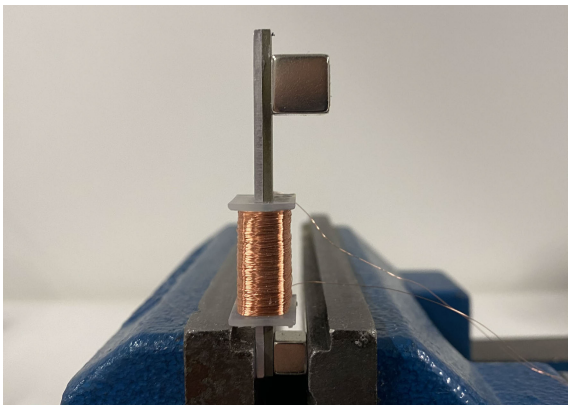

Fig. 9. Magnetostrictive energy harvester for experiments.

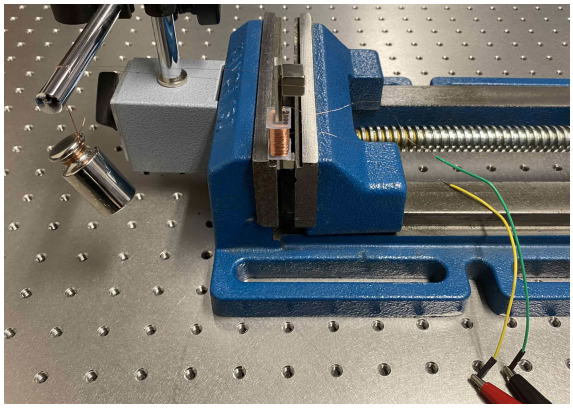

(a)

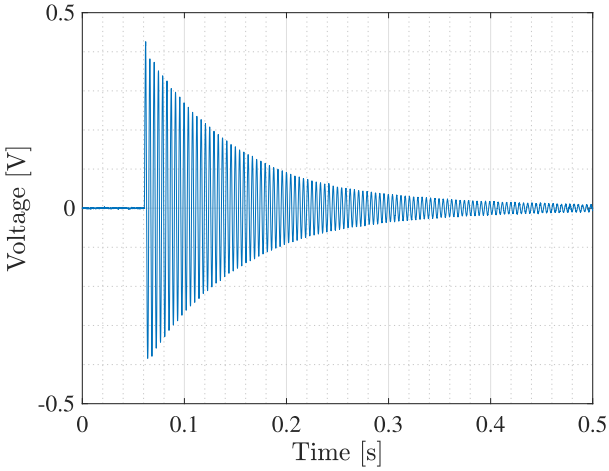

(b)

Fig. 10. Free vibration experiment to measure natural frequency ω_1 and damping ratio ζ_1 of cantilever. (a) Experimental setup. (b) Open-circuit free voltage response.

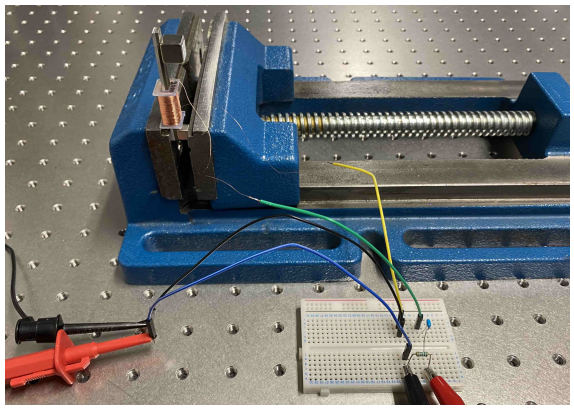

(a)

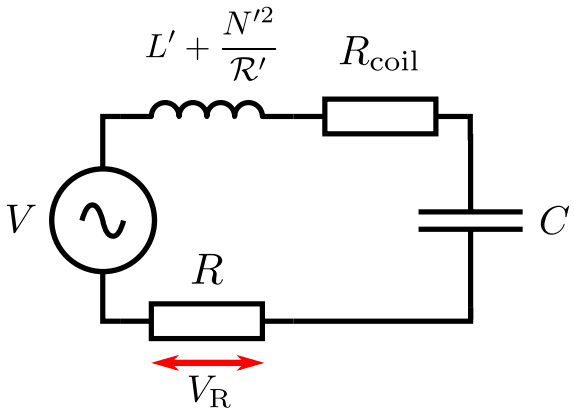

(b)

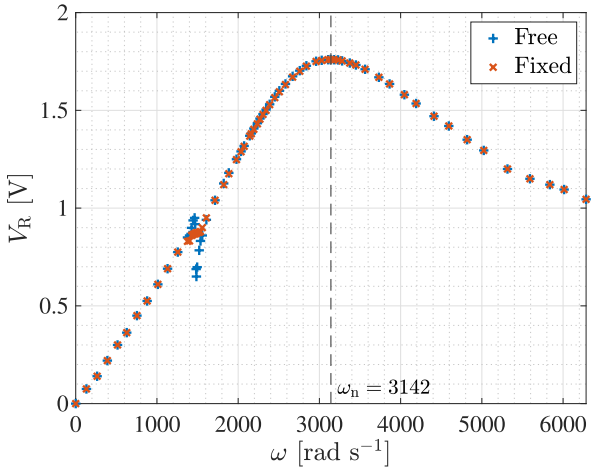

(c)

Fig. 11. Frequency response measurements to identify inductance $L' + (N'^2/\mathcal{R}')$. (a) Experimental setup. (b) Circuit diagram. (c) Frequency responses of voltage at resistive load.

The inductance $L' + (N'^2/\mathcal{R}')$ was identified from frequency response measurements. Fig. 11(a) and (b) shows the experimental setup and its circuit diagram, respectively. A series-resonant circuit was made by connecting a resistive load ($R = 99.4\ \Omega$), a capacitor ($C = 1.00\ \mu$F), and an ac voltage supply with 5 V to the pickup coil of the magnetostrictive energy harvester. In this series-resonant circuit, the amplitude of the voltage V_{R} at the load resistance is given

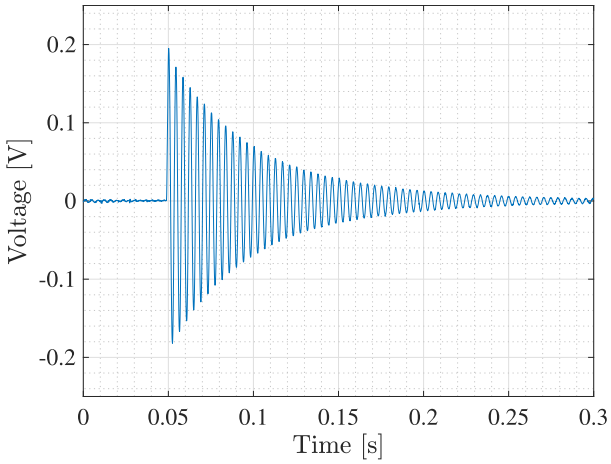

(a)

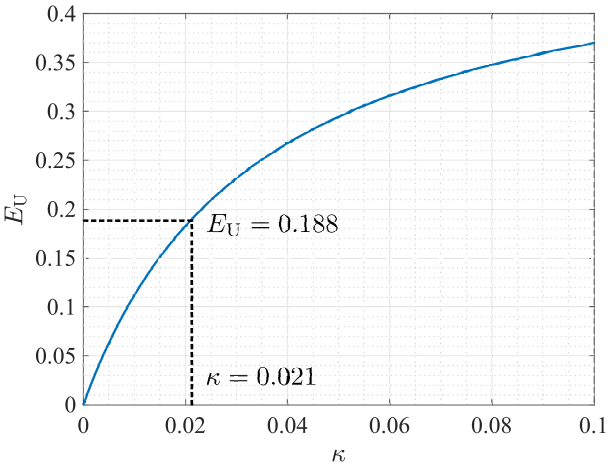

(b)

Fig. 12. Energy-harvesting efficiency measurement to estimate electromagnetic-mechanical spring constant ratio κ. (a) Free voltage response. (b) Analytical relationship between energy-harvesting efficiency E_{U} and electromagnetic-mechanical spring constant ratio κ based on (34).

as follows:

$$|V_{\text{R}}| = \frac{R}{\sqrt{\left[\frac{1}{\omega C} - \left(L' + \frac{N'^2}{\mathcal{R}'}\right)\omega\right]^2 + (R_{\text{coil}} + R)^2}}|V| \tag{46}$$

where V and ω are the voltage from the ac voltage supply and its frequency. From (46), it can be seen that regardless of the resistance values of the pickup coil and resistive load, the resonant frequency ω_{n} of the series-resonant circuit is determined by the values of the inductance and capacitance

$$\omega_{\text{n}} = \frac{1}{\sqrt{\left(L' + \frac{N'^2}{\mathcal{R}'}\right)C}}. \tag{47}$$

Therefore, the inductance can be obtained by measuring the resonant frequency ω_{n}. Fig. 11(c) shows the two types of frequency responses of the voltage V_{R} at the resistive load. The frequency responses were measured for two cases: One with the tip of the cantilever mechanically fixed to avoid the interaction with mechanical vibration, and the other without fixing the tip. Even though there is a clear difference between the two frequency responses around the resonance of

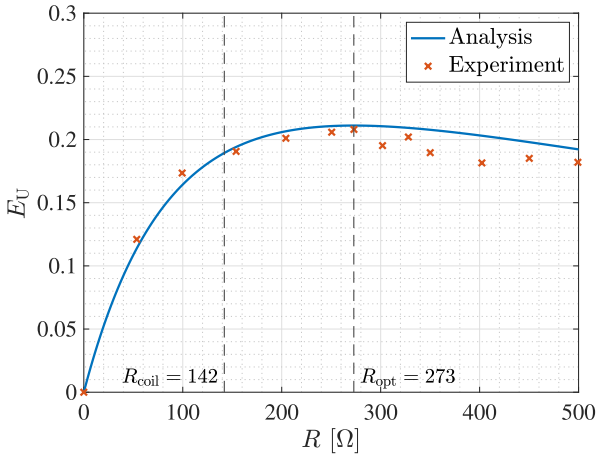

Fig. 13. Changes in energy-harvesting efficiency of magnetostrictive energy harvester with a pure resistive circuit.

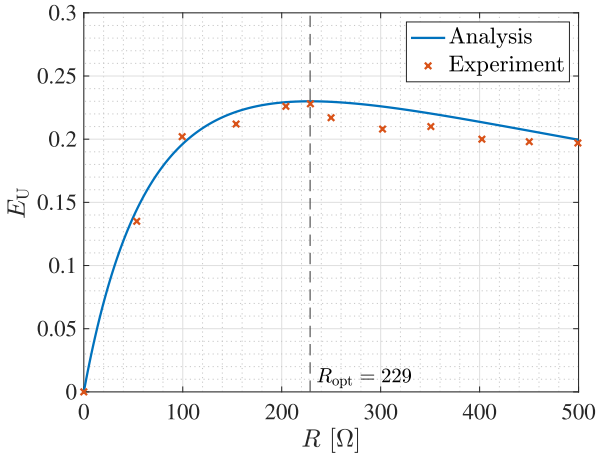

(a)

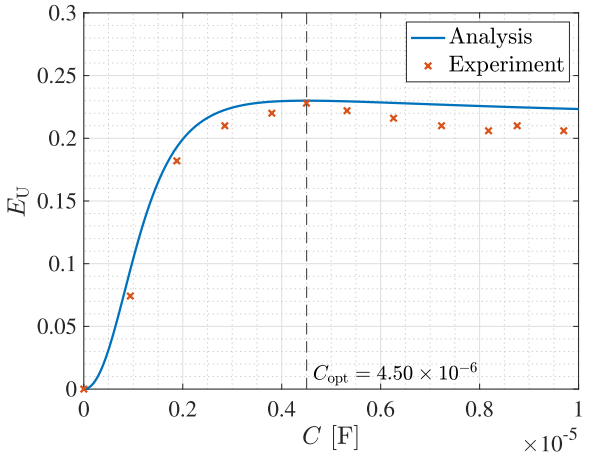

(b)

Fig. 14. Changes in energy-harvesting efficiency of magnetostrictive energy harvester with a series-resonant circuit. (a) Variation in load resistance R ($C = 4.50 \times 10^{-6}$ F. (b) Variation in capacitance C ($R = 229$ Ω).

the cantilever, both frequency responses show the electrical resonance at $\omega_n = 3142$ rad s^{-1}. Therefore, the inductance of the magnetostrictive energy harvester can be estimated as follows:

$$L' + \frac{N'^2}{\mathcal{R}'} = \frac{1}{\omega_n^2 C} = 0.101 \text{ H}. \tag{48}$$

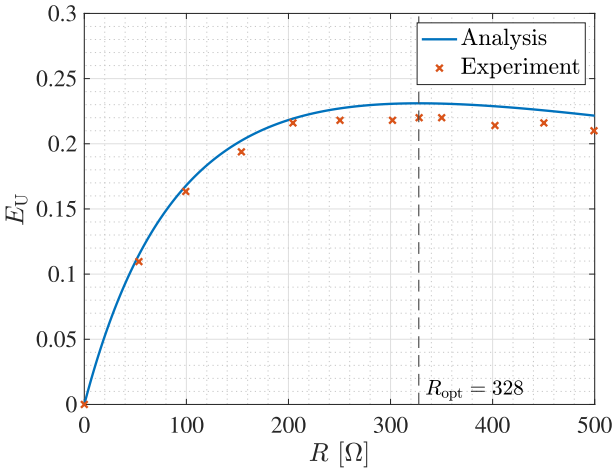

(a)

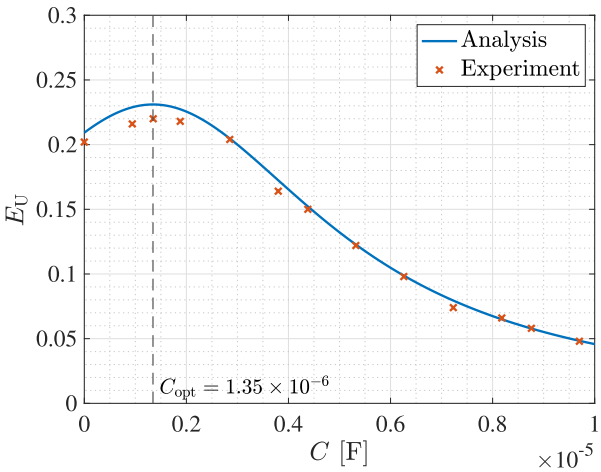

(b)

Fig. 15. Changes in energy-harvesting efficiency of magnetostrictive energy harvester with a parallel-resonant circuit. (a) Variation in load resistance R ($C = 1.35 \times 10^{-6}$ F. (b) Variation in capacitance C ($R = 328$ Ω).

The electromagnetic-mechanical spring constant ratio κ was estimated from the energy-harvesting efficiency of the magnetostrictive energy harvester connected to a pure resistive circuit with $R = 140$ Ω. The free vibration was induced by the 100 g weight. In the experiment, the energy-harvesting efficiency E_U was obtained as follows:

$$E_U = \frac{\int_0^\tau \frac{V_R^2}{R} dt}{\frac{1}{2}\left(k' - \frac{\theta^2}{\mathcal{R}'}\right) W_{mag}^2(0)} \tag{49}$$

where the spring constant is determined from the equilibrium of the forces

$$\left(k' - \frac{\theta^2}{\mathcal{R}'}\right) W_{mag}(0) = Mg \tag{50}$$

where M and g are the mass of the weight and gravity acceleration, respectively. τ is the finite time until the induced free voltage response is sufficiently damped. In this study, the free voltage response was integrated for $\tau = 5$ s. The initial displacement $W_{mag}(0) = 0.034$ mm was measured by a laser displacement sensor (optoNCDT 1900 from Micro-Epsilon). Fig. 12(a) shows the obtained free voltage response.

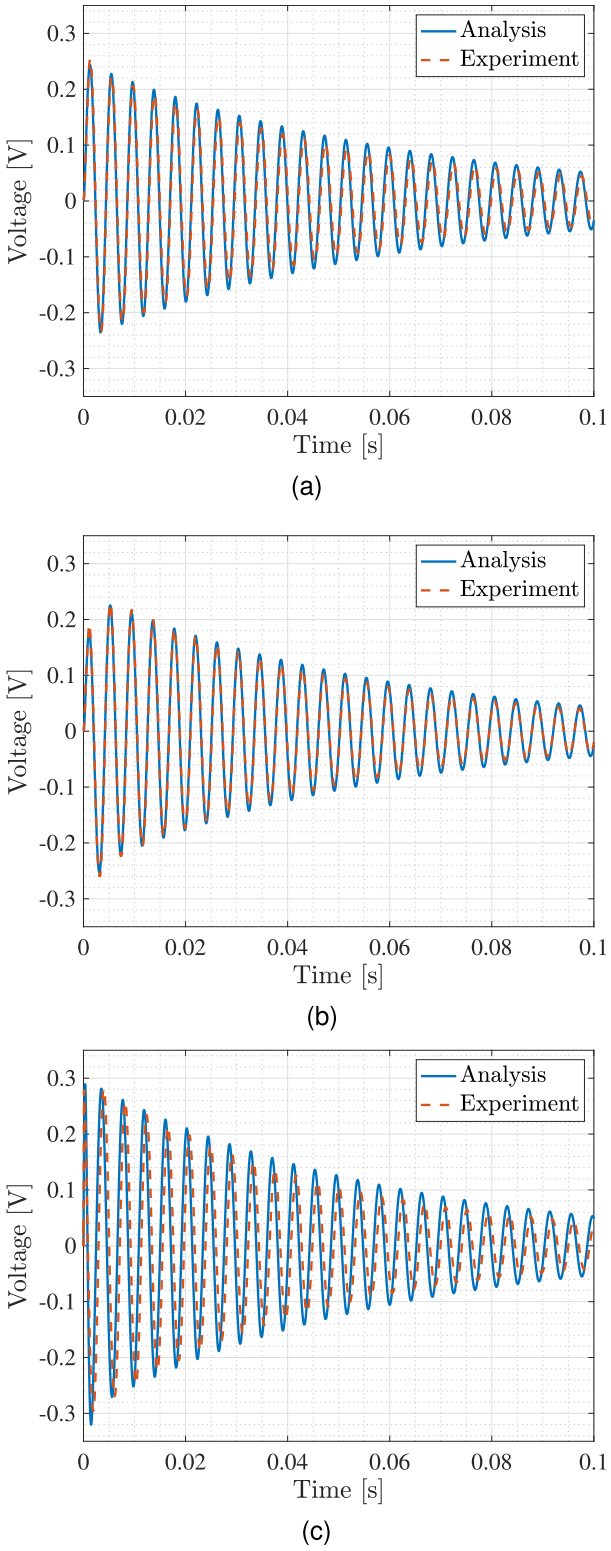

Fig. 16. Analytical and experimental free voltage responses with maximum energy-harvesting efficiencies. (a) Resistive. (b) Series. (c) Parallel.

From (49), $E_{\mathrm{U}} = 0.188$ was calculated. The energy-harvesting efficiency E_{U} is a monotonically increasing function with respect to the electromagnetic-mechanical spring constant ratio κ, thus there is only one κ corresponding to $E_{\mathrm{U}} = 0.188$. Fig. 12(b) shows the analytical relationship between E_{U} and κ based on (34). From (34), $\kappa = 0.021$ was estimated.

VI. Experimental Validation

The experimental validation was conducted by measuring the changes in the energy-harvesting efficiency (49) due to variations in the load resistance R and capacitance C, and comparing them with the analytical results. Fig. 13 shows the changes in energy-harvesting efficiency of the magnetostrictive energy harvester with a pure resistive circuit. The experimental results closely match the analytical results. According to the impedance matching, the optimal resistance value is expected to be equal to the coil resistance $R_{\mathrm{coil}} = 142\ \Omega$. However, both experimental and analytical results in this study revealed that the optimal resistance value is greater than the coil resistance. The analytical energy-harvesting efficiency at the optimal resistance $R_{\mathrm{opt}} = 273\ \Omega$ is $E_{\mathrm{U}} = 0.211$. Fig. 14(a) and (b) shows the changes in energy-harvesting efficiency of the magnetostrictive energy harvester with a series-resonant circuit due to variations in the load resistance R and capacitance C, respectively. There is a good agreement between the analytical results and experimental results, and the analytical results can estimate the optimal resistance and capacitance. The analytical maximum energy-harvesting efficiency of the series-resonant configuration is $E_{\mathrm{U}} = 0.230$. Fig. 15(a) and (b) shows the changes in energy-harvesting efficiency of the magnetostrictive energy harvester with a parallel-resonant circuit due to variations in the load resistance R and capacitance C, respectively. Similar to the case of the series-resonant circuit, the analytical results and experimental results have a good agreement. The analytical maximum energy-harvesting efficiency of this circuit configuration is $E_{\mathrm{U}} = 0.231$. Fig. 16(a)–(c) shows the analytical and experimental free voltage responses with the maximum energy-harvesting efficiencies. The analytical responses were calculated based on (25) and (39). In addition to the voltage amplitudes, their dampings show good agreement in all the configurations. Especially in the series-resonant configuration (Fig. 16(b)), the analytical response accurately produced the voltage drop in the initial wave of the response, which also strengthen the validity of the proposed analytical method.

VII. Conclusion

This article presented a method to maximize the energy-harvesting efficiency of the magnetostrictive energy harvester connected to a resonant circuit based on the linear and fundamental oscillation assumptions. The leakage magnetic flux from the coil acts as inductance, while the leakage flux from the magnetostrictive material acts to reduce the effective number of turns in the coil. Therefore, regardless of the presence of the magnetic flux leakage, energy-harvesting efficiency is uniquely described with five non-dimensional parameters that can be obtained from experiments. As a result, the magnetic flux leakage does not need to be considered.

This study investigated the optimal design parameters to maximize the energy-harvesting efficiency for two cases: one where the harvester is excited solely by kinetic energy and the other by potential energy. From the results, it was figured out that the optimal design parameters vary depending on the ratio of kinetic energy and potential energy within the given energy.

However, these optimal design parameters are approximately equal when the electromagnetic-mechanical spring constant ratio κ is sufficiently small.

In the magnetostrictive energy harvester connected to a series-resonant circuit, the design parameters to maximize the energy-harvesting efficiency to given kinetic energy were derived in extremely simple algebraic forms while the other optimal parameters are highly complex to be solved algebraically, and thus obtained numerically. It is noteworthy that the derived optimal natural frequency ratio $\nu_{\text{opt}} = 1$ is also the optimal value in several criteria [18], [19] for vibration suppression when the electromagnetic-mechanically coupled system is utilized as a dynamic vibration absorber, also known as a tuned mass damper.

The obtained analytical experimental results have shown that the magnetostrictive harvester connected to a resonant circuit is superior to the harvester connected to a pure resistive circuit regardless of whether a series or parallel configuration is used. The maximized energy-harvesting efficiencies of the series- and parallel-resonant configurations were 23.0% and 23.1%, respectively. Although the analytical calculations show a slightly higher efficiency for the parallel-resonant configuration, this study concludes that the magnetostrictive energy harvester with a series-resonant circuit is the best among the three circuit configurations considering its energy efficiency and simple algebraic optimal parameters.

ACKNOWLEDGMENT

This work was supported by the Research to Business Funding under Grant BFRK/2140/31/2023 (Awarded by Business Finland) and Grant 20230082 (Awarded by Walter Ahlström Foundation).

REFERENCES

[1] B. Christian, F. K. Chang, and Y. Fujino, *Encyclopedia of Structural Health Monitoring*. Chichester, U.K.: Wiley, 2009.

[2] T. Ueno, "Magnetostrictive vibrational power generator for battery-free IoT application," *AIP Adv.*, vol. 9, no. 3, Mar. 2019, Art. no. 035018.

[3] M. M. Ahmad, N. M. Khan, and F. U. Khan, "Review of frequency up-conversion vibration energy harvesters using impact and plucking mechanism," *Int. J. Energy Res.*, vol. 45, no. 11, pp. 15609–15645, Sep. 2021.

[4] X. Li, G. Hu, Z. Guo, J. Wang, Y. Yang, and J. Liang, "Frequency up-conversion for vibration energy harvesting: A review," *Symmetry*, vol. 14, no. 3, p. 631, 2022.

[5] S. Priya, "Modeling of electric energy harvesting using piezoelectric windmill," *Appl. Phys. Lett.*, vol. 87, no. 18, Oct. 2005, Art. no. 184101.

[6] Z. Lin and Y. Zhang, "Dynamics of a mechanical frequency up-converted device for wave energy harvesting," *J. Sound Vib.*, vol. 367, pp. 170–184, Apr. 2016.

[7] Y. Tan, G. Lu, M. Cong, X. Wang, and L. Ren, "Gathering energy from ultra-low-frequency human walking using a double-frequency up-conversion harvester in public squares," *Energy Convers. Manage.*, vol. 217, Aug. 2020, Art. no. 112958.

[8] T. Ueno and S. Yamada, "Performance of energy harvester using iron–gallium alloy in free vibration," *IEEE Trans. Magn.*, vol. 47, no. 10, pp. 2407–2409, Oct. 2011.

[9] R. A. Kellogg, A. B. Flatau, A. E. Clark, M. Wun-Fogle, and T. A. Lograsso, "Temperature and stress dependencies of the magnetic and magnetostrictive properties of $Fe_{0.81}Ga_{0.19}$," *J. Appl. Phys.*, vol. 91, no. 10, pp. 7821–7823, May 2002.

[10] J. Atulasimha and A. B. Flatau, "A review of magnetostrictive iron–gallium alloys," *Smart Mater. Struct.*, vol. 20, no. 4, 2011, Art. no. 043001.

[11] E. Lefeuvre, D. Audigier, C. Richard, and D. Guyomar, "Buck-boost converter for sensorless power optimization of piezoelectric energy harvester," *IEEE Trans. Power Electron.*, vol. 22, no. 5, pp. 2018–2025, Sep. 2007.

[12] L. Zuo and W. Cui, "Dual-functional energy-harvesting and vibration control: Electromagnetic resonant shunt series tuned mass dampers," *J. Vib. Acoust.*, vol. 135, no. 5, Oct. 2013, Art. no. 051018.

[13] S. Palumbo, P. Rasilo, and M. Zucca, "Experimental investigation on a Fe-Ga close yoke vibrational harvester by matching magnetic and mechanical biases," *J. Magn. Magn. Mater.*, vol. 469, pp. 354–363, Jan. 2019.

[14] Y. Mizukawa, U. Ahmed, M. Zucca, D. Blažević, and P. Rasilo, "Small-signal modeling and optimal operating condition of magnetostrictive energy harvester," *J. Magn. Magn. Mater.*, vol. 547, Apr. 2022, Art. no. 168819.

[15] Y. Mizukawa, U. Ahmed, D. Blažević, and P. Rasilo, "Modeling and efficiency maximization of magnetostrictive energy harvester under free vibration," *J. Sound Vib.*, vol. 558, Aug. 2023, Art. no. 117759.

[16] L. Wang and F. G. Yuan, "Vibration energy harvesting by magnetostrictive material," *Smart Mater. Struct.*, vol. 17, no. 4, Aug. 2008, Art. no. 045009.

[17] M. Safaei, H. A. Sodano, and S. R. Anton, "A review of energy harvesting using piezoelectric materials: State-of-the-art a decade later (2008–2018)," *Smart Mater. Struct.*, vol. 28, no. 11, Nov. 2019, Art. no. 113001.

[18] T. Ikegame, K. Takagi, and T. Inoue, "Exact solutions to H_∞ and H_2 optimizations of passive resonant shunt circuit for electromagnetic or piezoelectric shunt damper," *J. Vibrat. Acoust.*, vol. 141, no. 3, Jun. 2019, Art. no. 031015.

[19] T. Asami, Y. Mizukawa, and T. Ise, "Optimal design of double-mass dynamic vibration absorbers minimizing the mobility transfer function," *J. Vib. Acoust.*, vol. 140, no. 6, 2018, Art. no. 061012.